Flow Dynamics in Stented Ureter

Shaokai Zheng, Dario Carugo, Francesco Clavica, Ali Mosayyebi, and Sarah Waters

1 Introduction

Urinary flow is governed by the principles of fluid mechanics. Urodynamic investigations are frequently employed to diagnose lower urinary tract symptoms [1, 2], and many recent studies have focused on the fundamental flow dynamics of the ureter using fluid mechanical modelling methods, both theoretical and experimental [3]. Such studies have revealed the fundamental kinematics and dynamics of urinary flow in various physiological and pathological conditions, which are cornerstones for future development of diagnostic knowledge and innovative devices.

In a nutshell, there are three primary approaches to study the fluid mechanical characteristics of urinary flow: reduced order, computational, and experimental methods. Reduced-order methods exploit the disparate length scales inherent in the system to reveal the key dominant physics. Computational models can simulate

S. Zheng (✉) · F. Clavica
ARTORG Center for Biomedical Engineering Research, Faculty of Medicine, University of Bern, Bern, Switzerland
e-mail: shaokai.zheng@unibe.ch; francesco.clavica@unibe.ch

D. Carugo
Department of Pharmaceutics, UCL School of Pharmacy, University College London, London, United Kingdom
e-mail: d.carugo@ucl.ac.uk

A. Mosayyebi
Bioengineering Sciences, Faculty of Engineering and Physical Sciences, University of Southampton, Southampton, United Kingdom
e-mail: a.mosayyebi@soton.ac.uk

S. Waters
Oxford Centre for Industrial and Applied Mathematics, Mathematical Institute, University of Oxford, Oxford, United Kingdom
e-mail: sarah.waters@maths.ox.ac.uk

fully three-dimensional, time-dependent flows in physiologically-inspired anatomical domains. Finally, experimental models provide an excellent counterpart to reduced and computational models by providing physical tests under various physiological and pathological conditions.

2   Fundamental Characteristics of the Stented Ureter for Modelling Purposes

The key components of the human urinary system are illustrated in Fig. 1. The base flow is established by urine transport from the kidneys to the bladder. The generated urinary flow rates are in the order of 1 mL/min for each kidney [3], but can be higher or lower based on fluid intake or pathological conditions such as polyuria and diabetes mellitus.

For most fluid mechanical studies, the kidneys and bladder are treated as boundaries of the ureteric domain where pressure conditions are prescribed. The intraluminal renal pelvic pressure averages 12–15 cmH$_2$O [4, 5], and is generally considered to be below 20 cmH$_2$O for healthy individuals. The intraluminal renal pelvic pressure is often imposed as the inlet pressure boundary condition (BC) for ureteric flow models.

The bladder pressure is usually defined as the detrusor pressure, which is clinically measured by subtracting the intra-abdominal pressure from the intravesical pressure. The detrusor pressure remains small (roughly 2–5 cmH$_2$O) during the filling phase, but rises in the voiding phase, especially in men as a result of the extra resistance caused by the prostate. In a retrospective study of 976 healthy
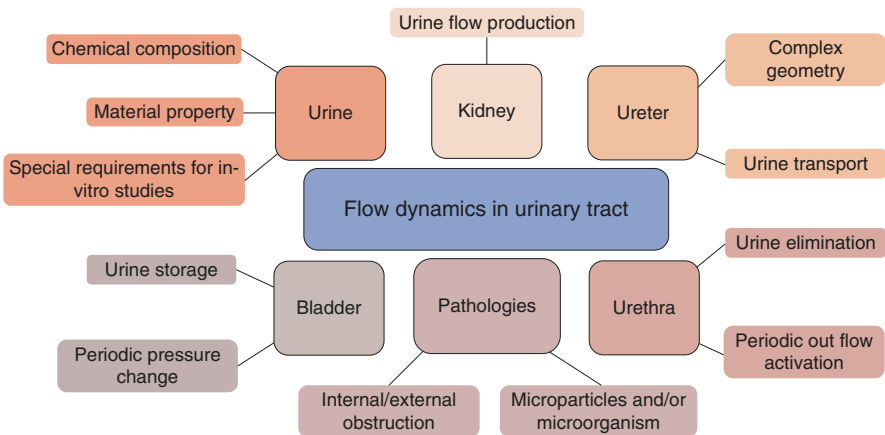

Fig. 1 Illustration of the key components of human urinary system and the primary considerations in designing a physiological model. For multi-organ models, connections between components need to be carefully addressed as well

individuals, the detrusor pressure at maximum flow rate during voiding was reported as 38.3 ± 11.5 cmH$_2$O for males and 32 ± 10.6 cmH$_2$O for females [6]. The voiding time of a normal bladder (capacity of approximately 500 mL) is around 40 s for healthy individuals [6]. The magnitude and duration of the pressures during filling and voiding can be used to specify the outlet condition of the ureteric domain, in contrast to explicitly including the bladder and urethra in the model.

The ureter is usually described as a tube of approximately 22–30 cm in length [7], and 1–6 mm in diameter [8]. The diameter is smaller at the ureteropelvic junction (UPJ), ureterovesical junction (UVJ), and where the ureters turn medially and cross the common iliac vessels. The ureter is typically modelled as either a straight or an undulated tube [9, 10].

Finally, to complete a model setup, characteristics of the stent need to be prescribed. This is straightforward for in-vitro studies at the macroscopic level, where commercially available stents can be directly used in the model ureter. For research into the fundamental physics, design parameters such as stent length, diameter (outer/inner), side hole arrangements (e.g. diameter, spacing, vertex angle), and material properties can be investigated at different scales (e.g. local behaviour in vicinity of side holes of varying geometries).

3 Reduced Models

Reduced-order methods are often employed to develop theoretical models of the flow dynamics within a (stented) ureter. Here we highlight the approaches adopted, and refer the interested reader to the review paper by Zheng et al. [3] for discussion of the details of the mathematical equations.

Lubrication theory was used to derive some of the earliest reduced models for the ureter [11–13], motivated by the small aspect ratio of the ureter (i.e. ratio of radius to length is small or R/L <<1) and the small reduced Reynolds number of ureteric flow (Re ~ 1). In the lubrication regime, the full Navier–Stokes equation was simplified to derive the urine flux and pressure distribution within a ureter subject to prescribed displacement of the ureter walls [11] to model the effects of peristalsis. The insertion of a catheter (or stent) was shown not to affect the pressure distribution within the ureter, providing confidence that urological pressure measurements made with a catheter are trustworthy [12].

Major limitations of the earliest models include the neglect of kidney and bladder activities, and the treatment of the catheter or stent as a solid tube without side holes, so that the permeability of the walls of the catheter or stent was neglected. This was ameliorated by Cummings et al. [14], where the kidney and bladder were treated with dynamic pressure BCs and the stent walls were assumed to be permeable. The ureter was considered to be a passive linearly-elastic tube that deformed in response to the transmural pressure across it. Their results indicate that during voiding the bladder pressure rises significantly and reflux can occur. Stents with higher permeability cause less total reflux than those with smaller permeability,

which suggests that more side holes can help reduce urine reflux. The model was further developed to incorporate more physiological descriptions of bladder pressure variation [15] (i.e. during voiding or spasms), a nonlinear elastic ureter wall law [15, 16], and the urine production from kidneys [16]. The authors argued that reflux exacerbates stent encrustation (primarily caused by the crystalline deposits of salts from urine) by returning bladder urine and bacteria to the ureter and renal pelvis. Increased duration of bladder spasm pulse and higher peak pressure during voiding were both shown to increase the total reflux, suggesting that patients should not squeeze hard during voiding, and the stent design should be optimized to reduce bladder irritations.

We note that peristalsis of the ureter wall can be strongly affected by the presence of an implanted ureteral stent, even ceasing completely, as concluded from several experiments using porcine models [17, 18] and a human patient study with indwelling double-J stent [19]. It is therefore common to neglect peristalsis in stented ureter models, especially for in-vitro investigations.

Finally, there have been models dealing with micro-particle laden (e.g. stone fragments or crystalline particles) urine flows. In this context, urine is modeled as a multiphase medium with solid particles [20–22]. In these models, the coupling is one way: the particles do not affect the flow dynamics, but the fluid flow governs the transport of the particles. The ureter is modeled as a two-dimensional channel with solid boundaries under peristaltic waves, and the fluid phase is solved by the Navier–Stokes equations. The effect of the fluid flow on particle transport is then determined by solution of the Basset–Boussinesq–Oseen equation. These methods are largely used to study particle trajectories and sedimentation under ureteric peristaltic waves. The exact results from these studies are therefore less relevant in the case of a stented ureter, since the peristaltic movement is largely impeded by the indwelling stent.

4   Computational Methods

While reduced models are useful to probe the underlying physics of the urinary system with minimal requirements for computational power, full computational models are able to simulate multiple configurations in clinically realistic settings by systematically varying physiological and stent-related parameters. Two solution techniques exist to solve full computational models. The conventional Computational Fluid Dynamic (CFD) approach solves only for the fluid domain and treats all solid components as prescribed BCs, whereas the Fluid–Structure Interaction (FSI) approach solves the governing equations for both the fluid and solid domains, coupled via conditions at the fluid–solid interface [23, 24].

CFD has been widely used to study design parameters of stents, such as number of side holes [9, 10, 25–27], inter-hole distance [10, 26, 27] and angular positions [10, 25–27] in various ureter shapes [10, 26] with different levels of ureteral obstructions [10, 25, 27, 28]. Results from straight ureter models showed that most of the

side holes are inactive (no through flow) in the absence of blockages [25], except perhaps the ones nearest to the UPJ or UVJ [10, 25]. With a local blockage present, the side holes in the vicinity of the blockage become increasingly active as the degree of blockage increases [25, 28]. Increasing the number of side holes (consequently decreasing the side hole interval) was shown to promote total flow rates [26, 27, 29], but the angular arrangement of side holes showed no impact on the total flow rate [27]. In the case of curved ureter models, the total flow rate was smaller compared to straight ureters [10], and the side holes were found to be active even in the absence of obstruction [26]. The stent wall thickness and the vertex angle of side holes were also studied in a CFD model of a microfluidic chip that replicated only a segment of the stented ureter [30]. Based on the local wall shear stress level, reducing stent wall thickness and adopting a 45° vertex angle for the side hole edges were proposed as strategies to reduce encrustation rates in inactive side holes.

The peristaltic movement of ureter wall is often omitted in CFD studies. In a few exceptions, a periodic wave of the ureter wall was prescribed and the effect of obstruction level was investigated [31, 32]. Nonetheless, the FSI method is more suitable for this type of study, where the ureter wall is modeled as a solid with appropriate constitutive equations capturing its material properties (e.g. elasticity). Previous FSI studies mainly focused on the characteristics of peristaltic waves such as maximum height, wave speed, and number of waves per ureter length [33, 34]. The proximal segment of the ureter was shown to suffer from a higher level of wall shear stress associated with a back flow at the beginning of peristalsis [33–35]. When an obstruction was introduced, higher shear stresses and pressure gradients were observed near the obstruction [36, 37]. Notably, a comparison between a full axisymmetric 3D ureter model and its corresponding 2D case showed negligible differences in shear stress and pressure gradient levels along the entire ureter length [36], and suggested that the simpler 2D axisymmetric model should be always considered first. Finally, in a study of a stented ureter [38], strains and stresses over the ureter obtained from a FSI study suggested a rigid-body behavior. The authors therefore recommended CFD as a cost efficient, but equally accurate option, for similar cases, where peristalsis is not considered.

5   Experimental Methods

In addition to providing physical insights, experimental models are also essential for the generation of data to calibrate and validate theoretical and computational models. Once validated by detailed comparison of theoretical model predictions with experimental data, theoretical and computational models can go beyond the experimental results by simulating more complex geometries and boundary conditions. Specifically, for the upper urinary tract (UUT), experimental studies have focused on the following aspects: (1) bacterial growth, (2) drainage capabilities of stents, and (3) the interplay between fluid mechanics and encrustation.

5.1 Bacterial Growth

Studies on bacterial growth in ureters aim to investigate encrustation and biofilm formation from a chemical and biological point of view. In the earliest studies [39, 40] on UUT, stents were not considered and the bladder was modelled as a static flask with periodic emptying cycles to simulate micturition. Volume capacity, residual volume and frequency of micturition were taken into account to study the bacterial susceptibility to antibiotics. It was demonstrated that the amount of bacteria in the urinary tract can be reduced with frequent micturition [39].

After stents were introduced in the clinical setting, several studies focused on investigating encrustation and biofilm growth in stented ureters. In general, different types of results can be achieved when static or dynamic models are used. Static models [41] were normally characterized by big reservoirs filled with artificial urine in which stents were immersed for a defined time interval. The results of these studies showed that 60% of the surface was covered by encrustation (mainly characterised by hydroxyapatite and struvite crystals) within 2 weeks, and that encrustation reached 100% coverage after 10 weeks.

Dynamic models were later introduced to overcome the main limitations of the static models and mimic more closely the physiological conditions. For example, filling and emptying cycles were introduced to model micturition which was not possible with static models. To this end, Chong et al. [42] introduced a syphon at the bladder outlet to automatically empty the bladder, when bladder volume reached a defined value (this volume could be controlled by changing the height of the syphon).

To facilitate comparison of stent designs, multi-testing platforms were introduced to enable simultaneous testing of several stent samples [43–45]. These experimental models were normally closed loops and constant urine flow was enforced by means of volumetric pumps (periodic bladder filling/emptying was not considered). Encrustation in dynamic models was found to be significantly lower than in static models, demonstrating the pivotal role of the flow on biofilm and encrustation growth.

5.2 Drainage Capabilities

Quantification of the drainage behaviour of ureteral stents is essential for assessing/ comparing stent performance. Hofmann and Hartung [46] used a reservoir to model the kidney and a 9-F (3 mm) polyvinyl tube with a stent inside (placed below the kidney) to model a stented ureter. To quantify the intraluminal drainage of stents, threads were tied around the polyvinyl tube to simulate obstructions. A similar approach was followed by Lange et al. [47] who used casted spheres to model ureteral obstructions. By keeping the head pressure constant, the performance of different stents were compared in terms of total flow rates [47]. A pressure driven flow setup was also adopted by Kim et al. [48]. In their experiments, stents of different diameters were inserted in silicone ureters. These ureter models closely mimicked the architecture of real human ureters as their geometry was based on computed tomographic (CT) scans from

patients. Curved ureters were compared with simplified straight ureters in their study. These experiments showed that higher hydraulic resistance is associated with bigger stents (i.e., stents with higher diameters) and curved ureters [48].

In contrast to the pressure-driven flows highlighted above, Olweny et al. [49] adopted a flow-driven approach to quantify the drainage properties of ureteral stents: constant flow was enforced and the pressure difference across the stent samples was measured. The hydraulic resistance of each stent sample was calculated using Poiseuille's law. Their in-vitro results, however, did not match the associated in-vivo data, probably because of the morphological changes induced in the ureters by the presence of the indwelling stents.

In order to reproduce more physiologically realistic conditions, Graw and Engelhardt [50] provided an experimental setup to mimic ureteral peristalsis using 24 inflatable cuffs surrounding an inner tube which modelled the ureter (a thin-walled tube with four lobes). The peristaltic wave, causing the bolus propagation, was reproduced by periodically activating the pressure in each cuff. Their investigations allowed to measure the pressure waveform associated to the bolus propagation; few suggestions were also provided to help the selection of catheters for intraluminal pressure measurements in ureters. Moreover, a bladder model reproducing the physiological pressure–volume curves was introduced by Kim et al. [51]. In their model, micturition was achieved using an outlet valve which opened at target pressure values. Measured peak bladder pressure, in this model, was found in the physiological range 20–80 cmH_2O (during micturition).

5.3   Interplay Between Fluid Mechanics and Encrustation

Flow-particle models investigate the interplay between fluid mechanics and encrustation/biofilm development in stented ureters (in addition to drainage capabilities of stents). Clavica et al. [52] and Carugo et al. [53] developed an in-vitro transparent model of the ureter based on measurements in porcine ureters. They quantified the relation between renal pressure and parameters including urine viscosity, urine flow rate, and level of obstruction. Notably, using fluorescent particles flowing in the transparent model, they were the first to provide flow visualisation in stented ureters and to observe the presence of laminar vortices near stent side-holes. It was hypothesised that these vortices can be anchoring sites for crystal and bacterial deposits [52, 53]. Following these findings, microfluidic 'stent-on-chip' models were developed by Mosayyebi et al. [54] to investigate intraluminal and extraluminal flows in stented ureters at the microscale level. In this study, flow streamlines at selected locations were obtained using fluorescent tracers and comparisons with computational equivalents were provided. An inverse correlation between particle accumulation and wall shear stress was identified. In further studies, the same research group investigated: (1) a novel side hole [30] with an optimised 'streamlined architecture' which led to lower particle deposition and (2) the influence of wall shear stress on bacterial adhesion [55]. Similarly to particle accumulation, it was found that low wall shear stress are associated with higher bacterial coverage.

6 Conclusion

In summary, this chapter has highlighted the various approaches established to study the flow dynamics in stented ureter. While the interdisciplinary approaches to date have provided a wealth of insight into the fluid mechanical properties of the stented ureter, the next challenge is to develop new theoretical, computational and experimental models to capture the complex interplay between the fluid dynamics in stented ureters and biofilm/encrustation growth. Such studies will (1) enable identification of clinically relevant scenarios to improve patients' treatment, and (2) provide physical guidelines for next-generation stent design.

References

1. Abrams P. Urodynamics. 3rd ed. London: Springer; 2006.
2. Griffiths D. Urodynamics: the mechanics and hydrodynamics of the lower urinary tract. Bristol: Adam Hilger in Collaboration with the Hospital Physicists Association; 1980.
3. Zheng S, Carugo D, Mosayyebi A, Turney B, Burkhard F, Lange D, et al. Fluid mechanical modeling of the upper urinary tract. WIREs Mech Dis. 2021;13:e01523.
4. Rattner William H, Fink S, Murphy JJ. Pressure studies in the human ureter and renal pelvis. J Urol. 1957;78(4):359–62.
5. Walzak MP, Paquin AJ. Renal pelvic pressure levels in management of nephrostomy. J Urol. 1961;85(5):697–702.
6. Alloussi SH, Lang C, Eichel R, Ziegler M, Stenzl A, Alloussi S. Urodynamical benchmarks: a retrospective analyses of 976 combined urodynamics with no pathological findings to evaluate standard values. Eur Urol Suppl. 2010;9(2):227.
7. Hickling DR, Sun T-T, Wu X-R. Anatomy and physiology of the urinary tract: relation to host defense and microbial infection. Microbiol Spectr. 2015;3(4):2012.
8. Zelenko N, Coll D, Rosenfeld AT, Smith RC. Normal ureter size on unenhanced helical CT. Am J Roentgenol. 2004;182(4):1039–41.
9. Kim K-W, Kim H-H, Choi YH, Lee SB, Baba Y, Suh S-H. Arrangement of side holes in a double J stent for high urine flow in a stented ureter. J Mech Sci Technol. 2020;34:949–54.
10. Kim H-H, Choi YH, Lee SB, Baba Y, Kim K-W, Suh S-H. Numerical analysis of the urine flow in a stented ureter with no peristalsis. Biomed Mater Eng. 2015;26(s1):S215–S23.
11. Lykoudis PS, Roos R. The fluid mechanics of the ureter from a lubrication theory point of view. J Fluid Mech. 1970;43(4):661–74.
12. Roos R, Lykoudis PS. The fluid mechanics of the ureter with an inserted catheter. J Fluid Mech. 1971;46(4):625–30.
13. Kiil F. Urinary flow and ureteral peristalsis. In: Lutzeyer W, Melchior H, editors. Urodynamics: upper and lower urinary tract. Berlin: Springer; 1973. p. 57–70.
14. Cummings LJ, Waters SL, Wattis JAD, Graham SJ. The effect of ureteric stents on urine flow: reflux. J Math Biol. 2004;49(1):56–82.
15. Waters S, Heaton K, Siggers J, Bayston R, Bishop M, Cummings L, et al. Ureteric stents: investigating flow and encrustation. Proc Inst Mech Eng Part H J Eng Med. 2008;222(4):551–61.
16. Siggers JH, Waters S, Wattis J, Cummings L. Flow dynamics in a stented ureter. Math Med Biol. 2009;26(1):1–24.
17. Kinn AC, Lykkeskov-Andersen H. Impact on ureteral peristalsis in a stented ureter. An experimental study in the pig. Urol Res. 2002;30(4):213–8.
18. Venkatesh R, Landman J, Minor SD, Lee DI, Rehman J, Vanlangendonck R, et al. Impact of a double-pigtail stent on ureteral peristalsis in the porcine model: initial studies using a novel implantable magnetic sensor. J Endourol. 2005;19(2):170–6.

19. Mosli Hisham A, Farsi Hasan MA, Al-Zimaity Mohammed F, Saleh Tarik R, Al-Zamzami MM. Vesicoureteral reflux in patients with double pigtail stents. J Urol. 1991;146(4):966–9.
20. Jiménez-Lozano J, Sen M, Corona E. Analysis of peristaltic two-phase flow with application to ureteral biomechanics. Acta Mech. 2011;219(1–2):91–109.
21. Rath H, Reese G. Peristaltic flow of non-Newtonian fluids containing small spherical particles. Arch Mech. 1984;36(2):263–77.
22. Riaz A, Sadiq MA. Particle–fluid suspension of a non-Newtonian fluid through a curved passage: an application of urinary tract infections. Front Phys. 2020;8:109.
23. Hirt CW, Amsden AA, Cook JL. An arbitrary Lagrangian–Eulerian computing method for all flow speeds. J Comput Phys. 1974;14(3):227–53.
24. Benra F-K, Dohmen HJ, Pei J, Schuster S, Wan B. A comparison of one-way and two-way coupling methods for numerical analysis of fluid–structure interactions. J Appl Math. 2011;2011:16.
25. Tong JCK, Sparrow EM, Abraham JP. Numerical simulation of the urine flow in a stented ureter. J Biomech Eng. 2006;129(2):187–92.
26. Kim KW, Choi YH, Lee SB, Baba Y, Kim HH, Suh SH. Numerical analysis of the effect of side holes of a double J stent on flow rate and pattern. Biomed Mater Eng. 2015;26:S319–S27.
27. Kim H-H, Choi YH, Lee SB, Baba Y, Kim K-W, Suh S-H. Numerical analysis of urine flow through the side holes of a double J stent in a ureteral stenosis. Technol Health Care. 2017;25(S1):63–72.
28. Carugo D, Zhang X, Drake JM, Clavica F, editors. Formation and characteristics of laminar vortices in microscale environments within an obstructed and stented ureter: a computational study. In Proceedings of the 18th International Conference on Miniaturized Systems for Chemistry and Life Sciences, MicroTAS; October 26–30, 2014; San Antonio, TX, USA. The Chemical and Biological Microsystems Society; 2014.
29. Kim KW, Choi YH, Lee SB, Baba Y, Kim HH, Suh SH. Analysis of urine flow in three different ureter models. Comput Math Methods Med. 2017;2017:5172641.
30. Mosayyebi A, Lange D, Yann Yue Q, Somani BK, Zhang X, Manes C, et al. Reducing deposition of encrustation in ureteric stents by changing the stent architecture: a microfluidic-based investigation. Biomicrofluidics. 2019;13(1):014101.
31. Najafi Z, Gautam P, Schwartz BF, Chandy AJ, Mahajan AM. Three-dimensional numerical simulations of peristaltic contractions in obstructed ureter flows. J Biomech Eng. 2016;138(10):101002.
32. Najafi Z, Schwartz BF, Chandy AJ, Mahajan AM. A two-dimensional numerical study of peristaltic contractions in obstructed ureter flows. Comput Methods Biomech Biomed Eng. 2018;21(1):22–32.
33. Vahidi B, Fatouraee N, Imanparast A, Moghadam AN. A mathematical simulation of the ureter: effects of the model parameters on ureteral pressure/flow relations. J Biomech Eng. 2011;133(3):031004–9.
34. Vahidi B, Fatouraee N. A biomechanical simulation of ureteral flow during peristalsis using intraluminal morphometric data. J Theor Biol. 2012;298:42–50.
35. Hosseini G, Ji C, Xu D, Rezaienia MA, Avital E, Munjiza A, et al. A computational model of ureteral peristalsis and an investigation into ureteral reflux. Biomed Eng Lett. 2018;8(1):117–25.
36. Takaddus AT, Chandy AJ. A three-dimensional (3D) two-way coupled fluid–structure interaction (FSI) study of peristaltic flow in obstructed ureters. Int J Numer Methods Biomed Eng. 2018;34(10):e3122.
37. Takaddus AT, Gautam P, Chandy AJ. A fluid–structure interaction (FSI)-based numerical investigation of peristalsis in an obstructed human ureter. Int J Numer Methods Biomed Eng. 2018;34(9):e3104.
38. Gómez-Blanco JC, Martínez-Reina FJ, Cruz D, Pagador JB, Sánchez-Margallo FM, Soria F. Fluid structural analysis of urine flow in a stented ureter. Comput Math Methods Med. 2016;2016:5710798.
39. O'Grady F, Pennington JH. Bacterial growth in an in vitro system simulating conditions in the urinary bladder. Br J Exp Pathol. 1966;47(2):152–7.
40. Greenwood D, O'Grady F. An in vitro model of the urinary bladder. J Antimicrob Chemother. 1978;4(2):113–20.

41. Tunney MM, Bonner MC, Keane PF, Gorman SP. Development of a model for assessment of biomaterial encrustation in the upper urinary tract. Biomaterials. 1996;17(10):1025–9.
42. Choong SKS, Wood S, Whitfield HN. A model to quantify encrustation on ureteric stents, urethral catheters and polymers intended for urological use. BJU Int. 2000;86(4):414–21.
43. Cauda V, Chiodoni A, Laurenti M, Canavese G, Tommasi T. Ureteral double-J stents performances toward encrustation after long-term indwelling in a dynamic in vitro model. J Biomed Mater Res Part B Appl Biomater. 2017;105(8):2244–53.
44. Gorman SP, Garvin CP, Quigley F, Jones DS. Design and validation of a dynamic flow model simulating encrustation of biomaterials in the urinary tract. J Pharm Pharmacol. 2003;55(4):461–8.
45. Hobbs T, Schultz LN, Lauchnor EG, Gerlach R, Lange D. Evaluation of biofilm induced urinary infection stone formation in a novel laboratory model system. J Urol. 2018;199(1):178–85.
46. Hofmann R, Hartung R. Ureteral stents—materials and new forms. World J Urol. 1989;7(3):154–7.
47. Lange D, Hoag NA, Poh BK, Chew BH. Drainage characteristics of the 3F MicroStent using a novel film occlusion anchoring mechanism. J Endourol. 2011;25(6):1051–6.
48. Kim K-W, Kim H-H, Choi YH, Lee SB, Baba Y. Urine flow analysis using double J stents of various sizes in in vitro ureter models. Int J Numer Methods Biomed Eng. 2020;3:e3294.
49. Olweny EO, Portis AJ, Afane JS, Brewer AV, Shalhav AL, Luszczynski K, et al. Flow characteristics of 3 unique ureteral stents: investigation of a Poiseuille flow pattern. J Urol. 2000;164(6):2099–103.
50. Graw M, Engelhardt H. Simulation of physiological ureteral peristalsis. Urol Int. 1986;41(1):1–8.
51. Kim J, Lee MK, Choi B. A study on the fluid mechanical urinary bladder simulator and reproduction of human urodynamics. Int J Precis Eng Manuf. 2011;12(4):679–85.
52. Clavica F, Zhao X, ElMahdy M, Drake MJ, Zhang X, Carugo D. Investigating the flow dynamics in the obstructed and stented ureter by means of a biomimetic artificial model. PLoS One. 2014;9(2):e87433.
53. Carugo D, Elmahdy M, Zhao X, Drake M, Zhang X, Clavica F, editors. An artificial model for studying fluid dynamics in the obstructed and stented ureter. In 35th Annual International Conference of the IEEE Engineering in Medicine and Biology Society (EMBC); July 3–7 2013; Osaka, Japan. IEEE; 2013. p. 5335–8.
54. Mosayyebi A, Yue QY, Somani BK, Zhang X, Manes C, Carugo D. Particle accumulation in ureteral stents is governed by fluid dynamics: in vitro study using a "stent-on-chip" model. J Endourol. 2018;32(7):639–46.
55. De Grazia A, LuTheryn G, Meghdadi A, Mosayyebi A, Espinosa-Ortiz JE, Gerlach R, et al. A microfluidic-based investigation of bacterial attachment in ureteral stents. Micromachines. 2020;11(4):408.